Biochemical and Biophysical Research Communications 456 (2015) 695–699

Contents lists available at ScienceDirect

Biochemical and Biophysical Research Communications

journal homepage: www.elsevier.com/locate/ybbrc

Solution structure of 6aJL2 and 6aJL2-R24G amyloidogenics light chain proteins

Roberto Maya-Martinez, Paloma Gil-Rodriguez, Carlos Amero *

Laboratorio de Bioquímica y Resonancia Magnética Nuclear, Centro de Investigaciones Químicas, Universidad Autónoma del Estado de Morelos, Cuernavaca, Mexico

ARTICLE INFO

Article history:
Received 24 November 2014
Available online 16 December 2014

Keywords:
Amyloidosis
Nuclear Magnetic Resonance
Immunoglobulin light-chain

ABSTRACT

AL amyloidosis is the most common amyloid systemic disease and it is characterized by the deposition of immunoglobulin light chain amyloid fibers in different organs, causing organ failure. The immunoglobulin light chain germinal line 6a has been observed to over-express in AL patients, moreover, it was observed that, out of these amyloidogenic proteins, 25% present a mutation of an Arg to Gly in position 24. *In vitro* studies have shown that this mutation produces proteins with a higher amyloid fiber propensity. It was proposed that this difference was due, in part, to the formation of a non-canonical structural element. In order to get a more detailed understanding of the structural and dynamic properties that govern the amyloid fibers formation process, we have determined the solution structure by NMR for the two constructs, showing that the difference in amyloid fibril formation is not due to sequence or structure.

1. Introduction

In order to function correctly, most proteins have to adopt a stable three-dimensional structure. However, in the cellular environment, the proteins may be subject to conditions that may lead to partial or total loss of their native conformation, promoting the formation of aggregates or amyloid fibrils [1–3]. Primary amyloidosis (AL) or light chain amyloidosis is a deadly disease, caused by the deposition of insoluble amyloid fibrils in organs, causing organ failure and eventually death. AL is the most common systemic amyloidosis and it is generated by an abnormally proliferation of monoclonal population of plasma cells that produce immunoglobulin light chains proteins (LC). Once the LCs are in the blood flow, the proteins misfold, form fibrils and deposit in tissues and organs, being kidneys, heart and liver the most frequently affected [4–6].

It has been found that the germ line lambda 6a over-expresses in patients with AL; also, it was observed that out of these amyloidogenic LC, 25% present a mutation of an Arg to Gly in position 24. *In vitro* studies have shown that this mutation produces LC proteins with a higher amyloid fiber propensity and lower stability [7–9]. It was proposed that this difference was due, in part, to the formation of a non-canonical germ line 6a structure in the CDR1 (residue 25–32) due to the R24G mutation [8,7].

In order to get a more detailed understanding of the structural and dynamic properties that govern the amyloid fibers formation process, we have determined the solution structure by NMR for the two constructs: the light chains lambda 6a germ-line protein (6aJL2) and its single point mutation at position 24 (6aJL2-R24G). Surprisingly, we found that the mutant does not form the non-canonical structure predicted in solution, moreover, the two solution structures are very similar.

2. Materials and methods

2.1. Sample preparation

The recombinant proteins were expressed from the plasmids 6a/pet-27 and 6a-R24G/pet-27 transformed into *Escherichia coli* BL21(DE3) cells, grown at 37 °C in 1 L of 2XYT medium supplemented with 60 μg/mL kanamycin at 200 rpm. When the cells reached an OD_{600} of 0.9, they were transferred to 250 mL of minimal M9 media containing 1 g/L $^{15}NH_4Cl$ and 2 g/L of $^{13}C_6$-glucose (CIL) as the sole nitrogen and carbon sources supplemented with 60 μg/mL kanamycin [10]. After 1 h at 37 °C, the cells were induced by adding of 0.8 mM isopropyl-D-thiogalactoside (IPTG) and then grown at 25 °C at 100 rpm for 12 h before harvesting by centrifugation at 4000 rpm for 20 min.

The protein was extracted by osmotic shock with 20% (w/v) cold sucrose, in a buffer 100 mM Tris, pH 8.0 and 1 mM EDTA and

Abbreviations: NMR, Nuclear Magnetic Resonance; HSQC, heteronuclear single quantum correlation spectroscopy; NOE, nuclear Overhauser effect; Al amyloidosis, primary amyloidosis or light chain amyloidosis.

* Corresponding author at: Av. Universidad 1001, Col. Chamilpa, Cuernavaca, Morelos C.P. 62209, Mexico.

E-mail address: carlosamero@uaem.mx (C. Amero).

http://dx.doi.org/10.1016/j.bbrc.2014.12.044
0006-291X/

centrifuged at 4000 rpm. The pellet was resuspended with 20 mL of cold water and centrifuged at 4000 rpm for 25 min. The supernatant was purified by gel filtration (Hi-load 16/600 Superdex S-200 GE) with a buffer 50 mM Sodium Phosphate, pH 7.4 and 75 mM NaCl. Fractions containing the protein were combined and concentrated using a 3 kDa cutoff concentrator. Protein concentration was estimated by OD_{280} with an extinction coefficient of 14,565 M^{-1} cm^{-1} determined by PROTPARAM [11]. The approximate concentration for the samples was 1–2 mM.

2.2. NMR spectroscopy

NMR data were collected at 25 °C on a Varian 700 MHz VNMR-S spectrometer equipped with a cryogenically-cooled triple resonance pulsed field gradient probe at the Laboratorio Nacional de Estructuras de Macromoleculas (LANEM). Backbone resonance assignments for 6aJL2 were obtained using triple resonance experiments HNCA, HNCACB, CBCA(CO)NH, HNCACO and HNCO. Side-chain resonance assignments were obtained from 3D $^{1}H–^{15}N$-TOCSY (t_m = 50 ms), and HCCH-TOCSY. Distance restraints were obtained from 3D ^{15}N-edited NOESY-HSQC (t_m = 150 and 300 ms) and ^{13}C-edited NOESY-HSQC (t_m = 150 ms) spectra recorded in samples dissolved in 5% and 100% D_2O, respectively.

Whereas backbone resonance assignments for 6a-R24G were obtained from BMRB 15276 [12], transferred to a pH 7.4 and confirmed from an HNCACB and HNCO, side-chain resonance assignments were confirmed from 3D $^{1}H–^{15}N$-TOCSY (t_m = 50 ms) and HC-HSQC. Distance restraints were obtained from 3D ^{15}N-edited NOESY-HSQC (t_m = 150 ms) and ^{13}C-edited NOESY-HSQC (t_m = 150 ms) spectra recorded in samples dissolved in 5% and 100% D_2O, respectively. NMR data were processed and analyzed using NMRPipe [13], CARA [14] and in-house scripts.

2.3. Structural determination

NOE derived distance restraints from NOESY cross peak intensities were calculated using a calibration curve assuming distance proportional to $1/r^6$. Backbone torsion angle restraints were obtained from analyses of the H, N, Ca and Cb chemical shifts with TALOS+ [15]. Hydrogen bond restraints were inferred from Solvent Expose Amide experiments and Hydrogen/Deuterium exchange experiments.

Structure calculations were performed using simulated annealing protocols within the XPLOR-NIH software suite [16]. The two cysteines were linked together through upper distance restrains 2.12 Å and used through all the calculations. An initial set of structures was generated using a set of NOE restraints filtered from the X-ray structure of 6aJL2 (PBD: 2W0K [17]) with a cutoff of 10 Å, in addition to H-bonds and dihedral angle restraints. A final set of the 20 lowest energy structures were selected from 100, and subsequently refined by explicit water using restrained molecular dynamics in XPLOR-NIH [16] and linked together the disulfide bridge. Analysis of structures was done using XPLOR-NIH and PROCHECK-NMR [18].

2.4. Accession code

The assigned chemical shifts for 6aJL2 and 6aJL2-R24G at pH 7.4 have been deposited in the BioMagResBank under accession numbers 19870 and 19798, respectively.

The solution structure and NMR restrains for 6aJL2 and 6aJL2-R24G have been deposited in the PDB (http://www.pdb.com) under accession numbers 2MMX and 2MKW, respectively.

3. Results

Fig. 1AB shows the two dimensional $^{1}H–^{15}N$ correlated spectrum of 6aJL2 and 6aJL2-R24G recorded at 25 °C and pH 7.4; both spectra are very similar and present good dispersion and quality. The 6aJL2 spectra contains 91 of the 105 expected resonances (excluding the 6 prolines residues). Whereas the 6aJL2-R24G spectra contains 94 of the 105 expected proton resonances (excluding the 6 prolines residues). Residues that did not have H–N signal for both proteins were N1, F2, H8, R40, G58, S69, S70, S96, V100,

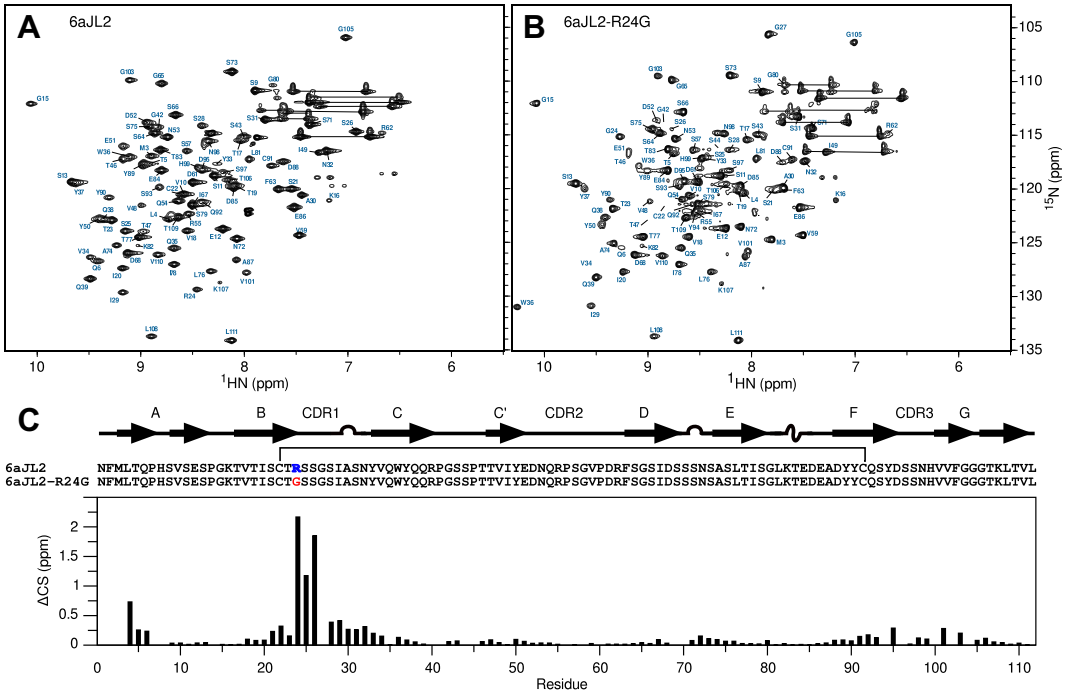

Fig. 1. Two dimensional $^{1}H–^{15}N$ HSQC spectra at pH 7.4 and 25 °C of (A) 6aJL2 and (B) 6aJL2-R24G. Backbone amide assignments are indicated. (C) Chemical shift differences as a function of residues. Sequences and secondary structure elements as found in the solution structures are shown.

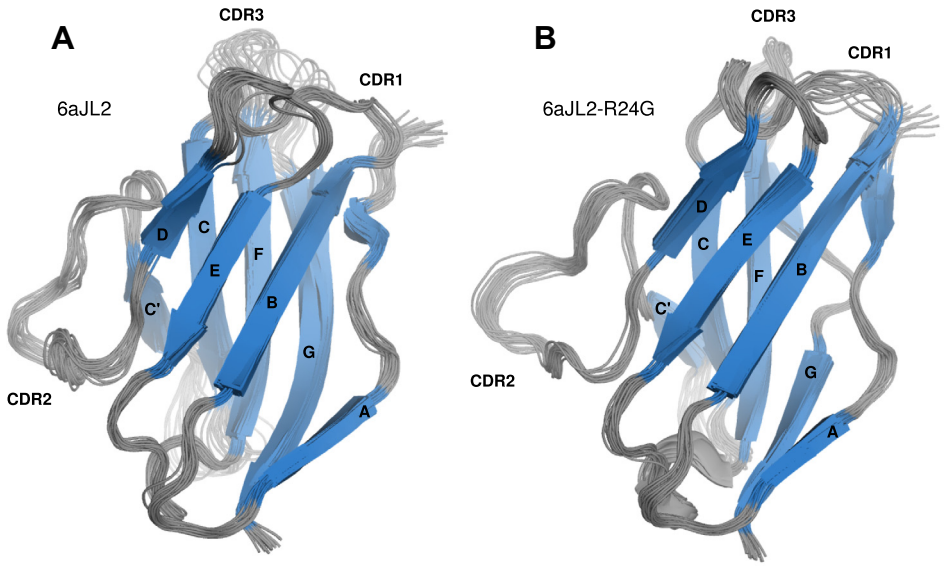

Fig. 2. Ensemble of 20 lowest-energy structures superposed on the backbone heavy atoms of (A) 6aJL2 and (B) 6aJL2-R24G. Images were rendered with PYMOL.

F102, and G104, probably due to solvent exchange (some of these residues were assigned at lower pH [12]). Residues S44 and Y94 present no signal for 6aJL2 and a minimal signal for 6aJL2-R24G, whereas residue G27 is not present in the germ line while it has a strong signal in the mutant, probably due to a change in dynamics.

Backbone amide resonance (H, N, CA, CB, and CO) assignments for 6aJL2 could be obtained for all of the observed signals corresponding to 90.1% of the protein, whereas, for 6aJL2-R24G, 92.5% of the backbone amide resonance assignments were obtained.

The effect of the mutation Arg to Gly at position 24 on the chemical shifts is shown in Fig. 1C. The largest differences correspond to signals from residues in the immediate vicinity of the mutation; residues 22–33 at the loop connecting strand B and C, and residues 4–6 at the N-termini. Most of the other signals are very similar, which suggested that the structures would be similar.

Table 1
NMR structure statistics.

NMR constrains	2MMX	2MKW
NOE	1216	1343
Intraresidue (i – j = 0)	535	471
Sequential (i – j = 1)	283	399
Medium range (1 < i – j < 5)	81	77
Long range (i – j < 5)	317	396
Hydrogen bonds[a]	31	31
Dihedral angles	189	200
Violations		
Distance violations >0.5 Å	0	0
Dihedral angle violations >5°	0	0
Deviation from idealized geometry		
Bonds, Å	2.61×10^{-3}	2.24×10^{-3}
Angles, °	0.51	0.46
Impropers, °	0.34	0.295
Ramachandran statistics, %		
Most favored region	81.3 ± 3.6	84.5 ± 2.9
Additional allowed region	15.5 ± 3.4	13.3 ± 2.4
Generously allowed region	2.9 ± 0.6	1.9 ± 1
Disallowed region	0.38 ± 0.5	0.33 ± 0.5
Structure precision[b]		
Backbone atoms, Å	0.74 ± 0.18	0.53 ± 0.09
Residues 4–40,44–90,100–109	0.52 ± 0.09	0.45 ± 0.07
All heavy atoms, Å	1.05 ± 0.25	0.93 ± 0.14

[a] Hydrogen bond were applied between amide proton and oxygen atoms, and between amide nitrogen and oxygen atoms for each restraint.
[b] RMS deviations are from the average structure.

The solution structure of both proteins could be determined and are well defined with a mean RMSD backbone deviation for the 6aJL2 of 0.74 Å and for the 6aJL2-R24G of 0.53 Å (Fig. 2). Overall, the structural quality is good, with more than 96% of the ψ and ϕ angles falling within the favored and additionally allowed regions of the Ramachandran plot for both proteins (Table 1).

The structured region of the proteins consists of two beta sheets with eight strands (Sheet 1: strand A: 3–12, strand B: 17–23, strand D: 63–67 and strand E: 72–78. Sheet 2: strand C: 34–39, strand C′: 46–50, strand F: 87–94 and strand G: 100–110) while the CDRs (Complementarity Determining Regions: CDR1: 25–31, CDR2: 51–54 and CDR3: 95–99) consist of hairpins providing the scaffold for the recognition.

Comparison of the structural elements from the NMR ensemble for 6aJL2 and 6aJL2-R24G reveals an overall backbone RMSD of 0.89 Å, with most of the structural difference in the loops that connect the beta strands. The crystal structure for the germ line has been reported by X-ray crystallography (PDB: 2W0K [17]), superposition of the solution structure and the X-ray structure lead to an RMSD of 0.83 Å, with the largest difference at residues 26–28 and residues 68–71. While the superposition of the structural elements from the NMR ensemble of the mutant 6aJL2-R24G and the 6aJL2 crystal structure leads to an RMSD of 0.56 Å, showing that the global structure of the mutant and the germ line are equals.

Even though globally both structures are very similar and we did not find specific NOEs that constrain completely the position of the Arg 24, which suggests that the side-chain undergoes some type of motion, probably the mutation eliminates relevant interactions. These presumably transient interactions, including a cation–pi with Phe 2, an ionic interaction with Asp 93 and some h-bonds, could easily explain the lower stability in the mutant protein.

Unexpectedly, the CDR1 of 6aJL2-R24G structure shows the same folding as the structure of 6aJL2 (PDB: 2W0K) and other members of the families 6a like WIL (PDB: 2CD0) and JTO (PDB: 1CD0) [19]. Therefore, it appears that the mutation at position 24 induces only slight structural changes in the protein, in clear contrast to what was been proposed before.

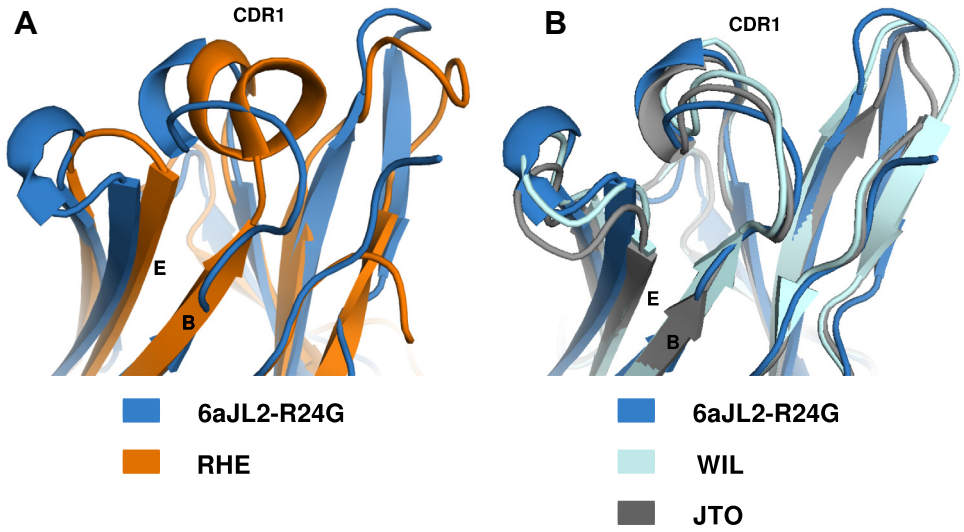

Fig. 3. Superposition of the CDR1 structural elements of a representative member from the NMR ensemble 6aJL2-R24G with (A) structure from RHE from germ line 1 and (B) X-ray structure from WIL and JTO members of the 6a family. Images were rendered with PYMOL.

4. Discussion

While the reported thermodynamics parameters for the germ line 6aJL2 and the 6aJL2-R24G mutant are different, showing a decrease in the stability of about 1.4 kcal/mol and a reduction for the melting temperature (t_m) from 49.9 to 44.2 °C [8], it is still difficult to understand how this single mutation drastically changes the fibril formation propensities, going for a lag time of about 14 h to a lag time of 2 h for the mutant. Moreover, there are some examples for this germ line in which proteins with the same stability have different amyloid fibril formation propensities [20].

To investigate if the substitution in the sequence at position 24 for an Arg to Gly has an effect in the amyloid propensity sequence-wise, we use the MetAmyl server [21]. This meta-predictor makes use of nine different algorithms to evaluate the sequence propensity to form amyloid fibrils giving back a consensus sequences. The consensus amyloidogenic regions for both proteins were the same; residues 17–22, 30–38, 46–51, 74–80 and 98–104. Therefore, it is reasonable to consider that, sequence-wise, the mutation by itself does not contribute to the increase in the amyloidogenic differences between the two proteins.

It was predicted, based in sequences alignments with structures for different germ lines, that the characteristic non-helical conformation for germ line lambda VI proteins was determined by the presence of an Arg residue in position 24. And therefore a Gly at this position would imply a different conformation for the CDR1, mimicking structures from germ lines that did not have an Arg, and the structural rearrangement would provoke the fibril formation differences.

Superposition of the NMR structure of 6aJL2-R24G and the crystal structure from RHE (PDB: 2RHE), a member of germ line 1 [22,23], reveals that the predicted helix element for the mutant was not formed (Fig. 3A). Moreover, the superposition with different members of the germ line 6a (JTO and WIL [19]) clearly shows that the 6aJL2-R24G mutant conserves the structure elements of the family (Fig. 3B). Nevertheless, it is still possible that the mutation eliminates some important interactions, due to the change of the size of the side-chain and the charge, that could be important in the protein stability.

Interestingly, even though the structures are very similar, the NOE patterns and intensities show small but relevant differences for both constructs, with more intense signals for 6aJL2-R24G. This fact could suggest a different dynamic behavior between the two proteins and could be related to the amyloid propensities. Further studies will be required to determine if there is a difference in the dynamics of 6aJL2 and 6aJL2-R24G and if this has an implication in the amyloid fiber formation process. Such studies should help reveal some of the features for the fibril formation.

We have obtained a family of NMR structures of the 6aJL2 and 6aJL2-R24G proteins. While the exact reason for the difference between the amyloid fibril propensity for the two proteins remains to be determined, we have demonstrated that the structural elements for these two constructs are maintained. This result was somehow unexpected because it has been assumed that some of the differences observed in amyloid fibril propensities were due to structural differences induced by the mutation at position 24. The solution structure of 6aJL2-R24G has allowed us to confirm that the mutation does not induce a helix element in the CDR1. These results suggest that the difference in the fibril formation propensities are not structurally or sequentially determined. Further characterization of dynamics for both constructs may provide useful information about the changes in molecular motion accompanying the mutation and may ultimately lead to a description for the amyloid propensities changes.

Acknowledgments

We thank Dr. Baltazar Becerril and Dr. Alejandro Fernandez for plasmids. Dr. Nina Pastor and group for assistance and helpful discussions. This work was supported by CONACYT Mexico Grant (CB-151780). This study made use of the LANEM facilities at CIQ-UAEM.

References

[1] F. Chiti, C.M. Dobson, Protein misfolding, functional amyloid, and human disease, Annu. Rev. Biochem. 75 (2006) 333–366, http://dx.doi.org/10.1146/annurev.biochem.75.101304.123901.
[2] V.N. Uversky, A.L. Fink, Conformational constraints for amyloid fibrillation: the importance of being unfolded, Biochim. Biophys. Acta 1698 (2004) 131–153, http://dx.doi.org/10.1016/j.bbapap.2003.12.008.
[3] D.S. Eisenberg, M. Jucker, The amyloid state of proteins in human diseases, Cell 148 (2012) 1188–1203, http://dx.doi.org/10.1016/j.cell.2012.02.022.
[4] M. Ramirez-Alvarado, Amyloid formation in light chain amyloidosis, Curr. Top. Med. Chem. 12 (2012) 2523–2533.
[5] A. Dispenzieri, M.a. Gertz, F. Buadi, What do I need to know about immunoglobulin light chain (AL) amyloidosis?, Blood Rev 26 (2012) 137–154, http://dx.doi.org/10.1016/j.blre.2012.03.001.

[6] G. Palladini, R.L. Comenzo, The challenge of systemic immunoglobulin light-chain amyloidosis (Al), Subcell. Biochem. 65 (2012) 609–642, http://dx.doi.org/10.1007/978-94-007-5416-4_22.
[7] L. del Pozo Yauner, E. Ortiz, B. Becerril, The CDR1 of the human lambdaVI light chains adopts a new canonical structure, Proteins 62 (2006) 122–129, http://dx.doi.org/10.1002/prot.20779.
[8] L. del Pozo-Yauner, E. Ortiz, R. Sánchez, R. Sánchez-López, L. Güereca, C.L. Murphy, et al., Influence of the germline sequence on the thermodynamic stability and fibrillogenicity of human lambda 6 light chains, Proteins 72 (2008) 684–692, http://dx.doi.org/10.1002/prot.21934.
[9] T. Mishima, T. Ohkuri, A. Monji, T. Kanemaru, Y. Abe, T. Ueda, Residual structures in the acid-unfolded states of Vlambda6 proteins affect amyloid fibrillation, J. Mol. Biol. 392 (2009) 1033–1043, http://dx.doi.org/10.1016/j.jmb.2009.07.078.
[10] J. Marley, M. Lu, C. Bracken, A method for efficient isotopic labeling of recombinant proteins, J. Biomol. NMR 20 (2001) 71–75. http://www.ncbi.nlm.nih.gov/pubmed/11430757.
[11] E. Gasteiger, C. Hoogland, A. Gattiker, S. Duvaud, M.R. Wilkins, R.D. Appel, et al., Protein Identification and Analysis Tools on the ExPASy Server, in: J. Walker (Ed.), Humana Press, 2005.
[12] L.H. Gutiérrez-González, L. Muresanu, L. del Pozo-Yauner, R. Sánchez, L. Guereca, B. Becerril-Luján, et al., (1)H, (13)C and (15)N resonance assignment of 6aJL2(R25G), a highly fibrillogenic lambdaVI light chain variable domain, Biomol. NMR Assign. 1 (2007) 159–161, http://dx.doi.org/10.1007/s12104-007-9045-9.
[13] F. Delaglio, S. Grzesiek, G.W. Vuister, G. Zhu, J. Pfeifer, A. Bax, NMRPipe: a multidimensional spectral processing system based on UNIX pipes, J. Biomol. NMR 6 (1995) 277–293. http://www.ncbi.nlm.nih.gov/pubmed/8520220.
[14] R.L.J. Keller, The Computer Aided Resonance Assignment Tutorial, CANTINA Verlag, 2004.
[15] Y. Shen, F. Delaglio, G. Cornilescu, A. Bax, TALOS+: a hybrid method for predicting protein backbone torsion angles from NMR chemical shifts, J. Biomol. NMR 44 (2009) 213–223, http://dx.doi.org/10.1007/s10858-009-9333-z.
[16] C. Schwieters, J. Kuszewski, G. Mariusclore, Using Xplor–NIH for NMR molecular structure determination, Prog. Nucl. Magn. Reson. Spectrosc. 48 (2006) 47–62, http://dx.doi.org/10.1016/j.pnmrs.2005.10.001.
[17] A. Hernández-Santoyo, L. del Pozo Yauner, D. Fuentes-Silva, E. Ortiz, E. Rudiño-Piñera, R. Sánchez-López, et al., A single mutation at the sheet switch region results in conformational changes favoring lambda6 light-chain fibrillogenesis, J. Mol. Biol. 396 (2010) 280–292, http://dx.doi.org/10.1016/j.jmb.2009.11.038.
[18] R. Laskowski, J.A. Rullmann, M. MacArthur, R. Kaptein, J. Thornton, AQUA and PROCHECK-NMR: programs for checking the quality of protein structures solved by NMR, J. Biomol. NMR 8 (1996), http://dx.doi.org/10.1007/BF00228148.
[19] P.R. Pokkuluri, A. Solomon, D.T. Weiss, F.J. Stevens, M. Schiffer, Tertiary structure of human lambda 6 light chains, Amyloid 6 (1999) 165–171. http://www.ncbi.nlm.nih.gov/pubmed/10524280 (accessed 15.10.14).
[20] J.S. Wall, V. Gupta, M. Wilkerson, M. Schell, R. Loris, P. Adams, et al., Structural basis of light chain amyloidogenicity: comparison of the thermodynamic properties, fibrillogenic potential and tertiary structural features of four Vlambda6 proteins, J. Mol. Recogn. 17 (2004) 323–331, http://dx.doi.org/10.1002/jmr.681.
[21] M. Emily, A. Talvas, C. Delamarche, MetAmyl: a METa-predictor for AMYLoid proteins, PLoS One 8 (2013), http://dx.doi.org/10.1371/journal.pone.0079722.
[22] C. Chothia, A.M. Lesk, Canonical structures for the hypervariable regions of immunoglobulins, J. Mol. Biol. 196 (1987) 901–917. http://www.ncbi.nlm.nih.gov/pubmed/3681981 (accessed 14.10.14).
[23] W. Furey, B.C. Wang, C.S. Yoo, M. Sax, Structure of a novel Bence-Jones protein (Rhe) fragment at 1.6 Å resolution, J. Mol. Biol. 167 (1983) 661–692. http://www.ncbi.nlm.nih.gov/pubmed/6876161 (accessed 15.10.14).